HIGH-ORDER IMPLICIT UNSTRUCTURED METHOD FOR COMPRESSIBLE FLOWS

Carlos Breviglieri, carbrevi@yahoo.com.br
Instituto Tecnológico de Aeronáutica, CTA/ITA/IEC, 12228-900, São José dos Campos, SP, Brazil

João Luiz F. Azevedo, azevedo@iae.cta.br
Instituto de Aeronáutica e Espaço, CTA/IAE/ALA, 12228-903, São José dos Campos, SP, Brazil

Abstract. *The purpose of this work is to extend the capabilities for high resolution spatial discretization methods of the unstructured code developed by the authors. The current code holds implementations of ENO and WENO schemes up to fourth order. As the intrinsic reconstruction model of these non-oscillatory schemes relies on gathering neighboring cells, or stencils, for polynomial reconstruction, such schemes were found to be very demanding on computer resources for resolution orders greater than three, in 2-D, or anything greater than 2nd order, in 3-D. This fact motivated the consideration of the Spectral Finite Volume method, as proposed by Wang et al., which is implemented in a cell centered finite volume context on triangular unstructured meshes for two dimensional models. This method is expected to perform better than ENO and WENO schemes, compared to the overall cost of the simulation, since it differs on the reconstruction model applied and it is currently extensible up to 4th-order accuracy. A comparative study of limiting methods is presented for the high-order SFV scheme. Also, the results are compared to those of low-order schemes and experimental data available in the literature.*

Keywords: *Spectral Finite Volume, Implicit Method, High Order Discretization, 2D Euler Equations, Unstructured Meshes*

1. INTRODUCTION

The Computational Aerodynamics group of Instituto de Aeronáutica e Espaço (IAE) has been developing CFD solvers for two and three dimensional systems, considering both structured and unstructured meshes for over a decade Basso *et al.* (2003). One research area of the development effort is aimed at the implementation of high-order methods suitable for problems of interest to the Institute, i.e., external high-speed aerodynamics. Some upwind schemes such as the van Leer flux vector splitting scheme van Leer (1982), the Liou AUSM$^+$ flux vector splitting scheme Liou (1996) and the Roe flux difference splitting scheme Roe (1981) were implemented and tested for second-order accuracy with a MUSCL reconstruction Anderson *et al.* (1986). However, the nominally second-order schemes presented results with an order of accuracy smaller than expected in the solutions for unstructured grids. Aside from this fact, it is well known that total variation diminishing (TVD) schemes have their order of accuracy reduced to first order in the presence of shocks due to the effect of limiters.

This observation has motivated the group to study and to implement essentially non-oscillatory (ENO) and weighted essentially non-oscillatory (WENO) schemes in the past Wolf and Azevedo (2006). However, as the intrinsic reconstruction model of these schemes relies on gathering neighbouring cells for polynomial reconstructions for each cell at each time step, both schemes were found to be very demanding on computer resources for resolution orders greater than three, in 2-D, or anything greater than 2nd order, in 3-D. This fact motivated the consideration of the spectral finite volume method, as proposed by Wang and co-workers Wang (2002); Wang and Liu (2002, 2004); Wang *et al.* (2004); Liu *et al.* (2006); Sun *et al.* (2006), as a more efficient alternative. The numerical solver is currently implemented for the solution of the 2-D Euler equations in a cell centered finite volume context for triangular meshes, with an implicit LU-SGS scheme for time integration.

The remainder of the paper is organized as follows. In section 2. the theoretical formulation is detailed. Section **??** presents the numerical formulation regarding the spatial and time integration methods. Details are given for linear, quadratic and cubic polynomial reconstructions for triangular mesh elements. Next, the high-order boundary representation and limiter formulation are discussed. In section 5 numerical results are presented and discussed.

2. THEORETICAL FORMULATION

2.1 Governing Equations

In the present work, the 2-D Euler equations are solved in integral form as

$$\frac{\partial}{\partial t}\int_V Q dV + \int_V (\nabla \cdot \vec{P}) dV = 0\,, \tag{1}$$

where $\vec{P} = E\hat{\imath} + F\hat{\jmath}$. The application of the divergence theorem to Eq. (1) yields

$$\frac{\partial}{\partial t}\int_V Q dV + \int_S (\vec{P}\cdot\vec{n}) dS = 0\,. \tag{2}$$

The vector of conserved variables, Q, and the convective flux vectors, E and V, are given by

$$Q = \left\{ \begin{array}{c} \rho \\ \rho u \\ \rho v \\ e_t \end{array} \right\}, \quad E = \left\{ \begin{array}{c} \rho u \\ \rho u^2 + p \\ \rho uv \\ (e_t + p)u \end{array} \right\}, \quad F = \left\{ \begin{array}{c} \rho v \\ \rho uv \\ \rho v^2 + p \\ (e_t + p)v \end{array} \right\}. \tag{3}$$

The standard CFD nomenclature is being used here. Hence, ρ is the density, u and v are the Cartesian velocity components in the x and y directions, respectively, p is the pressure, and e_t is the total energy per unit volume. The system is closed by the equation of state for a perfect gas

$$p = (\gamma - 1)\left[e_t - \frac{1}{2}\rho(u^2 + v^2)\right], \tag{4}$$

where e_t is the total energy per unit volume, and the ratio of specific heats, γ, is set as 1.4 for all computations in this work. In the finite volume context, for stationary meshes, Eq. (2) can be rewritten for the i-th mesh element as

$$\frac{\partial Q_i}{\partial t} = -\frac{1}{V_i}\int_S (\vec{P}\cdot\vec{n}) dS\,, \tag{5}$$

where Q_i is the cell averaged value of Q at time t and V_i is the volume, or area in 2-D, of the i-th mesh element.

3. NUMERICAL FORMULATION

For a given order of spatial accuracy using the SFV method, each SV_i element must be partitioned in

$$N_m = \frac{k(k+1)}{2} \tag{6}$$

sub-elements or control volumes (CVs). The evaluation of the conserved variables at the quadrature points is necessary in order to perform the flux integration over the mesh element faces. These evaluations can be achieved by reconstructing conserved variables in terms of some base functions using the DOFs within a SV. The present work has carried out such reconstructions using polynomial base functions, although one can choose any linearly independent set of functions. Let P_m denote the space of m-th degree polynomials in two dimensions. Then, the minimum dimension of the approximation space that allows P_m to be complete is

$$N_m = \frac{(m+1)(m+2)}{2}. \tag{7}$$

In order to reconstruct q in P_m, it is necessary to partition the SV into N_m non-overlapping CVs, such that

$$SV_i = \bigcup_{j=1}^{N_m} CV_{i,j}. \tag{8}$$

The reconstruction problem, for a given continuous function in SV_i and a suitable partition, can be stated as finding $p_m \in P_m$ such that

$$\int_{CV_{i,j}} p_m(x,y) dS = \int_{CV_{i,j}} q(x,y) dS. \tag{9}$$

With a complete polynomial basis, $e_\ell(x,y) \in P_m$, it is possible to satisfy Eq. (9). Hence, p_m can be expressed as

$$p_m = \sum_{\ell=1}^{N_m} b_\ell e_\ell(x,y), \tag{10}$$

where e is the base function vector, $[e_1, \cdots, e_{N_m}]$, and b is the reconstruction coefficient vector, $[b_1, \cdots, b_{N_m}]^T$. When one expresses the polynomial in terms of shape functions, $L = [L_1, \cdots, L_{N_m}]$, defined as $L = eS^{-1}$, where S represents the partition reconstruction matrix, as in Breviglieri *et al.* (2008), it is possible to write

$$p_m = \sum_{j=1}^{N_m} L_j(x,y) q_{i,j} = Lq. \tag{11}$$

Table 1. Polynomial base functions.

Reconstruction Order	e
linear	$[\,1\ x\ y\,]$
quadratic	$[\,1\ x\ y\ x^2\ xy\ y^2\,]$
cubic	$[\,1\ x\ y\ x^2\ xy\ y^2\ x^3\ x^2y\ xy^2\ y^3\,]$

Equation (11) gives the value of the conserved state variable, q, at any point within the SV and its boundaries, including the quadrature points, (x_{rq}, y_{rq}). The above equation can be interpreted as an interpolation of a property at a point using a set of cell averaged values and the respective weights, which are set equal to the corresponding cardinal base value evaluated at that point. Moreover, the polynomial base functions for the linear, quadratic and cubic reconstructions are listed in Table 1. For more details regarding partition quality and stability analysis the interested reader is referred to Refs. Breviglieri *et al.* (2008) and van den Abeele and Lacor (2007).

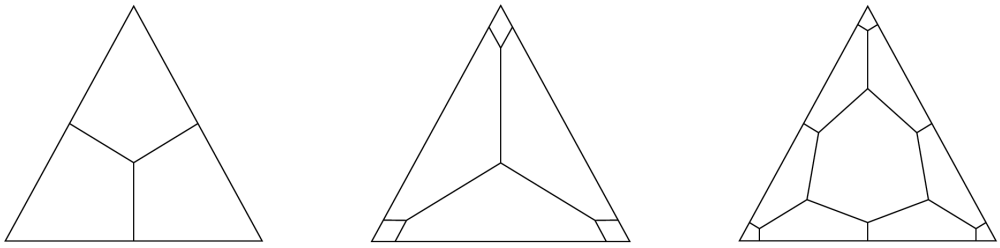

(a) (b) (c)

Figure 1. Triangular spectral volume partitions for (a) linear, (b) quadratic and (c) cubic reconstructions.

3.1 High-Order Boundary Treatment

From the formulation described thus far, it is clear that any input mesh will be divided into a finer mesh and, in principle, render the computation more costly. In the standard 2nd-order MUSCL finite volume scheme, the mesh boundaries are represented as line segments. This coarse approximation of the geometry results in a cluster of mesh nodes into highly-curved boundaries simply to represent the curved nature of it, in regions such as the leading edge of an airfoil, for instance.

If such approach is carried over to the SFV method, there is no gain in computational performance. As the literature presents for high-order schemes, such as Discontinuous Galerkin and SFV methods, one solution is to treat these boundary faces as curved from within the solver. For the present work, a quadratic and cubic boundary representation is performed for the 3rd and 4th-order SFV schemes. Although it is suggested to also perform a quadratic boundary representation to the 2nd-order SFV scheme Wang and Liu (2006) such approach is not followed here. Therefore, the 2nd order scheme has no special boundary treatment.

In order to perform this representation, one can adopt isoparametric SV elements and map them to the boundary data. However, this particular SV will differ in the partition design from the other SVs. Thus, it will require a dedicated reconstruction and shape function values for properties interpolation. In this work, only SV that are adjacent to wall boundaries receive this treatment.

Once the "curved" SV is partitioned, the interpolation shape functions and the CV face normals must be recalculated. Note that typically only one face of the SV stands at a boundary and one could use a simplified formulation for this specific face. For more information, the interested reader is referred to Ref. Wang and Liu (2006) and references therein.

4. High-Order Limiter Formulation

This section presents the high-order Parameter Free Generalized Hierarchical Moment Limiter formulation, or PFGHML for short. In the context of the Euler formulation, it is necessary to limit some reconstructed properties at flux integration points in order to maintain stability and convergence of the simulation, if the flow solution contains discontinuities. The present limiter technique involves two stages. First, the solver must find out and mark "troubled cells" which are, in the second stage, limited. For the detection and limiting process, the limiter employs a Taylor series expansion for the

reconstruction with regard to the cell-averaged derivatives. The troubled cells are, then, limited in a hierarchical manner, *i.e.*, from the highest-order derivative to the lowest-order one. If the highest derivative is not limited, the original polynomial is preserved and so is the order of the method at the element level. This limiter technique is capable of suppressing oscillations near solution discontinuities due to dispersion without loss of accuracy at local extrema in smooth regions. Originally, this limiter methodology was developed for the spectral difference method in Ref. Yang and Wang (2009). In the present work, the formulation is extended for the SFV method.

The quadratic limited polynomial, which is used in order to obtain property values at the quadrature points for a troubled SV_i spectral volume, is given by

$$\begin{aligned} p_i^{\text{limited}}(x_{rq}, y_{rq}) = Q_i &+ \phi_i^{(1)} \left[\frac{1}{V_i} \left(Q_x M_x + Q_y M_y \right)_i \right] \\ &+ \phi_i^{(2)} \left[\frac{1}{V_i} \left(\frac{1}{2} Q_{xx} M_{x^2} + Q_{xy} M_{xy} + \frac{1}{2} Q_{yy} M_{y^2} \right)_i \right] , \end{aligned} \tag{12}$$

where

$$M_{x^m y^n}|_i = \int_{SV} (x_{rq} - x_i)^m (y_{rq} - y_i)^n dV \tag{13}$$

represent the area moments of the cells. The x, xx, y, xy and other subscripts of Q denote derivatives with respect to x and y, while ϕ indicates the limiter function, all computed as indicated in Breviglieri *et al.* (2009). The limited reconstruction is based on primitive variables $\{\rho, u, v, p\}^T$, instead of conserved variables. Once these properties are available from the limited reconstruction, the vector of conserved variables is easily obtained to resume the numerical flux integration.

4.1 Temporal Discretization

In order to obtain the steady state solution of the flow from an initial condition, a relaxation scheme is necessary. The convergence behavior to steady state of high-order methods, such as the SFV method, is generally poor with explicit time marching approaches. The approach typically used in the present research group has been to resort to explicit, multi-stage, Runge-Kutta time-stepping methods. However, adequate solution convergence rate, especially for the higher-order implementations, dictate that an implicit time integrator should be employed. Therefore, an implicit LU-SGS scheme is also implemented in the context of the present work. Using an edge-based data structure, the Jacobian matrix is stored in lower, upper and diagonal components, which are computed as

$$\begin{aligned} L &= \frac{1}{2} \left[-J(q_{nb}, \vec{n}_r) - |\lambda| \, \mathbf{I} \right] \\ U &= \frac{1}{2} \left[J(q_{nb}, \vec{n}_r) - |\lambda| \, \mathbf{I} \right] \\ D &= \frac{V}{\Delta t} \mathbf{I} + \sum_{nb} \frac{1}{2} \left[J(q_i, \vec{n}_r) + |\lambda| \mathbf{I} \right] . \end{aligned} \tag{14}$$

where J is the Jacobian of the inviscid flux vectors in the direction normal to the edge and $|\lambda|$ represents a scalar dissipation model. Note that L, U and D represent the strict lower, upper and diagonal matrices, respectively. Equation (14) represents a system of linear simultaneous algebraic equations that needs to be solved at each time step. The iterative LU-SGS solution method is employed, along with a mesh renumbering algorithm Cuthill and McKee (1969), and the system is solved in two steps, a forward and backward sweep,

$$\begin{aligned} (D + L)\Delta q^* &= R \\ (D + U)\Delta q &= D\Delta q^* . \end{aligned} \tag{15}$$

More information about the current implicit method can also be found in Breviglieri *et al.* (2009).

5. NUMERICAL RESULTS

For the results here reported, density is made dimensionless with respect to the freestream condition and pressure is made dimensionless with respect to the freestream density times the freestream speed of sound squared. For the steady case simulations, the CFL number is set as a constant value and the local time step is computed using the local grid spacing and characteristic speeds. For all test cases, the CFL number is set to 10^{+6}.

All numerical simulations are carried out on a dual-core 3.0 GHz PC Intel64 architecture, with Linux OS. The code is written in Fortran 95 language and the Intel Fortran compiler® with optimization flags is used.

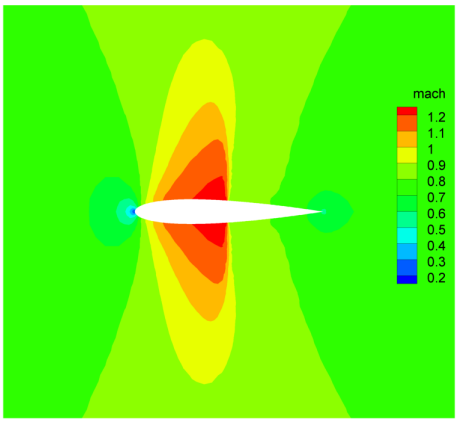

Figure 2. Mach contours of NACA 0012 transonic simulation obtained with the 2nd-order SFV method.

5.1 Limiter Effects

Throughout the development of the SFV method, various limiter formulations were considered, from the scalar conservation laws in Ref. Wang (2002) to the two and three dimensional system formulation in Refs Wang *et al.* (2004); Liu *et al.* (2006). Among these studies are the TVD and TVB methods also considering several limiting function. The current work initially resorted to the TVB and TVD limiter formulation as presented in the FV method to deal with the oscillations and instabilities of the SFV method. This section presents results of the earlier limiter models, namely the TVB methods, and also the latter proposed PFGHML limiter formulation. This is intended to give the reader a clear picture of the importance and necessity of the limiter formulation adopted for high-order method solutions.

Consider the test case of an external airfoil simulation with zero angle-of-attack and free stream Mach value of 0.8. At such configuration, a shock wave is expected to develop and be positioned half-way on both airfoil surfaces. This test case is similar to that presented later in section 5.3 The numerical results computed with the 2nd-order SFV method is presented in Fig. 2. The simulation is unstable and diverges when no limiter is employed. Hence, a TVB limiter was used to obtain this result. Figure 3 shows the same solution but now presents the CV mesh and highlights, in red, the cells for which the limiter is active at the last iteration considered. This figure clearly shows that the limiter function, here limiting the pressure reconstruction, is active on the shock wave region and close to the airfoil wall. Therefore, it is clear that the solution is no longer 2nd-order on those marked cells. The order reduction is obviously not desired. When the same test case is run with the 3rd-order SFV method, the limiter becomes much more “aggressive”, as shown in Fig. 4. Only those cells away from the airfoil and the shock region are not limited. Again, the limited cells are marked in red for the limited pressure reconstruction at the last iteration considered on this simulation. By considering these results, it becomes clear that there is no point in using a high-order method with conventional TVD and TVB limiter formulations.

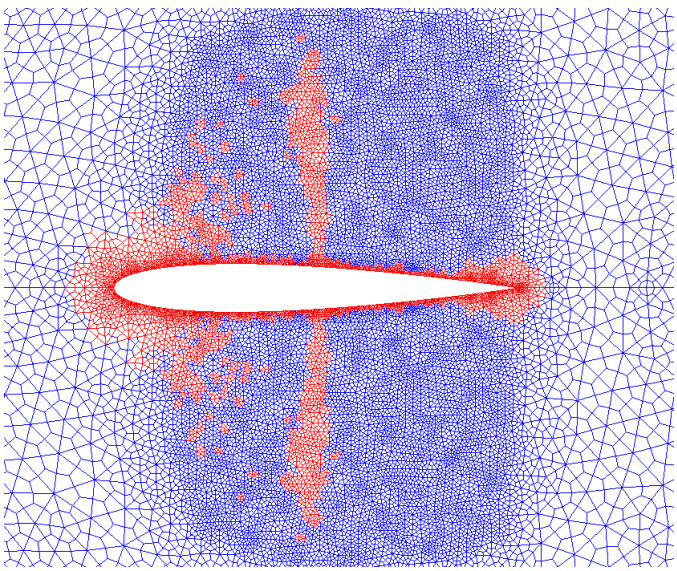

Figure 3. Limited cells (in red) for pressure reconstruction obtained with the 2nd-order SFV method with TVB limiter.

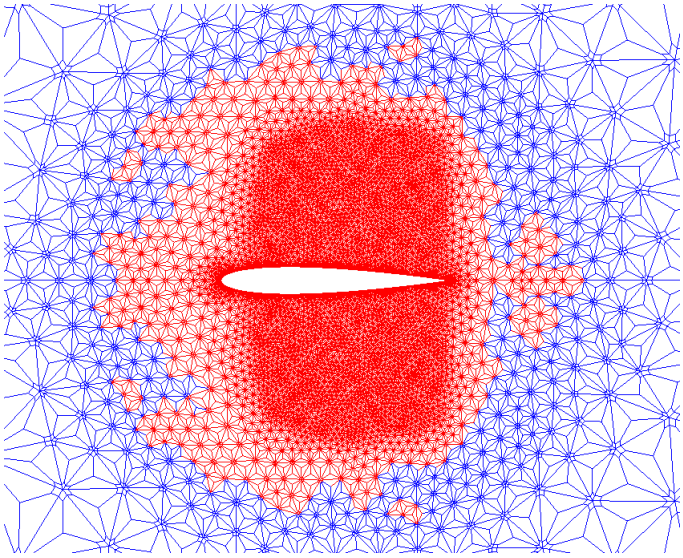

Figure 4. Limited cells (in red) for pressure reconstruction obtained with the 3rd-order SFV method with TVB limiter.

From these early results of the current research, it became clear to the author that a superior limiter formulation was required. The development of limiter formulations for high-order accurate methods are topics of intensive and recent research throughout the CFD community. For this work, the Parameter Free Generalized Hierarchical Moment Limiter formulation was developed. Results with the new formulation show a great improvement over the TVD and TVB formulations, in the sense that they mark as few as possible cells to perform the limited reconstruction. Results with the PFGHML limiter are presented in the following subsections.

5.2 Ringleb Flow

The Ringleb flow is an analytic solution of the compressible steady nonlinear Euler equations for a wall bounded flow. It represents an irrotational and isentropic flow around a symmetric blunt obstacle. This flow is interesting for several reasons. First, the wall geometry is a complex curve, resulting in a strong validation test of wall boundary conditions. Second, the flow itself is highly nonlinear, in some cases transitioning from subsonic to supersonic and back to subsonic without a shock.

Ringleb's flow is solved using a hodograph plane transformation. After expressing the momentum equations in stream function form, a solution can be obtained as

$$\Psi = \frac{1}{q}\sin\theta \tag{16}$$

where Ψ is the compressible stream function, q is the velocity magnitude, and θ is the flow angle measured from the x axis.

The flow is bounded by two streamlines, each defined by a constant value k. The value of k on the inner streamline is defined as $k_{\min}$, and the value of k on the outer streamline is denoted as $k_{\max}$. The geometry of the inflow and outflow boundaries are defined by a constant value of q, denoted as $q_{\max}$. In the present work, $k_{\min} = 0.4$, $k_{\max} = 0.8$ and $q_{\max} = 0.3$. The inflow boundaries normal vector is slightly modified to match the θ angle in order to preserve the velocity isolines of the problem.

Figure 5 shows the Ringleb's flow solution for Mach contours and the corresponding mesh. On a streamline, the maximum Mach number occurs at the $y = 0$ point, where $q = k$. An interesting feature of the Ringleb flow solution is that, due to the symmetry, a flow that becomes supersonic will decelerate to a subsonic velocity without forming a shock wave.

In order to measure the order of the implemented SFV method, four meshes are considered for the mesh refinement study, corresponding to 128, 512, 2048 and 8192 spectral volume elements. The analytical solution is computed for all meshes in order to measure how close the numerical results are to the exact solution. The error with respect to the analytical solution is computed using the L_1 and L_∞ norms of the density. Figure 5 shows the 2048-element grid and the Mach number contours computed in this grid with the fourth order SFV method, using the corresponding high-order boundary representation.

It should be pointed out that the same numerical test case was studied by the author in Ref. Breviglieri *et al.* (2008), considering only the linear boundary representation. It was observed in that effort that the low-order boundary treatment causes a shock wave to develop close to the inner boundary, which, then, makes the limiter active. Eventually, the shock

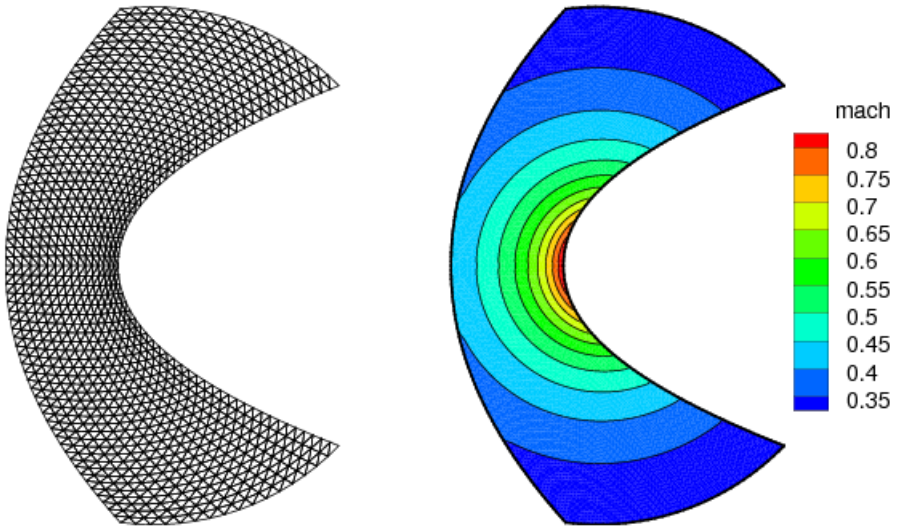

Figure 5. Ringleb flow mesh and Mach number contour results for fourth-order SFV method.

wave propagates and it causes the simulation to diverge. In the present work, however, which considers the higher-order boundary representation, reasonable results are always obtained for this test case, including the simulations with the fourth order SFV method. As previously discussed, for the third order scheme, a quadratic polynomial is used to represent the SV faces which lie along the geometry boundaries. In a similar fashion, for the fourth order scheme, a cubic polynomial is employed instead, which is compatible with the internal polynomial order of each SV. Figure 6 presents graphically the 3rd and 4th-order SFV method orders for this case. The actual orders of accuracy here obtained are in good agreement with the expected values. Therefore, it is safe to say that the current implementation of the SFV method is indeed high-order accurate.

5.3 NACA 0012 Airfoil

For the NACA 0012 airfoil simulation, one coarse mesh is considered. It has 716 cells and 358 nodes, from which 40 define the airfoil wall. This *O*-grid mesh is presented in Fig. 7. The airfoil profile itself is collapsed on the trailing edge. The far field boundary radius is 10 chord units.

The free stream flow replicate the conditions of the experimental data McDevitt and Okuno (1985), that is, free stream Mach number value of $M_\infty = 0.8$ and 0 deg angle-of-attack. Simulations with the second, third and fourth order SFV schemes are performed, along with the first-order Roe scheme. Figure 8 shows the computed Cp values obtained with with the first-order Roe scheme and third-order SFV method, considering quadratic curved boundaries. It is clear from the Cp distribution that the first-order scheme introduces too much dissipation and essentially smears out the shock wave. The high-order Cp distribution, on the other hand, is remarkably close to the experimental results in Fig. 8, particularly for the shock position, considering the crude mesh discretization. These show the potential for high-order methods, on such applications, to ease the mesh generation process. One should observe, however, that the experimental results consider the presence of the boundary layer and the consequent shock-boundary layer interaction that necessarily occurs in the experiment. For the numerical solution, the shock presents a sharper resolution, as one can expect for an Euler simulation.

Another relevant simulation is performed to assess the benefits of the curved boundary implementation, namely, the measure of entropy error ϵ_s levels at the airfoil boundary. Because the diffusive flux vectors are zero, there is no physical dissipation mechanism that produces heat in regions of smooth flow, away from shocks. If no external heat is added into the flow, then it is called adiabatic and, from the first law of thermodynamics, it follows that entropy, give by

$$s = C_v \ln\left(\frac{p}{\rho^\gamma}\right) , \tag{17}$$

is constant throughout the field if no shocks are present. Therefore, the entropy error ϵ_s, defined as

$$\epsilon_s = \frac{p}{p_\infty}\left(\frac{\rho_\infty}{\rho}\right)^\gamma - 1 , \tag{18}$$

is a good measure of the accuracy of a numerical solution obtained with a method to approximately solve the Euler

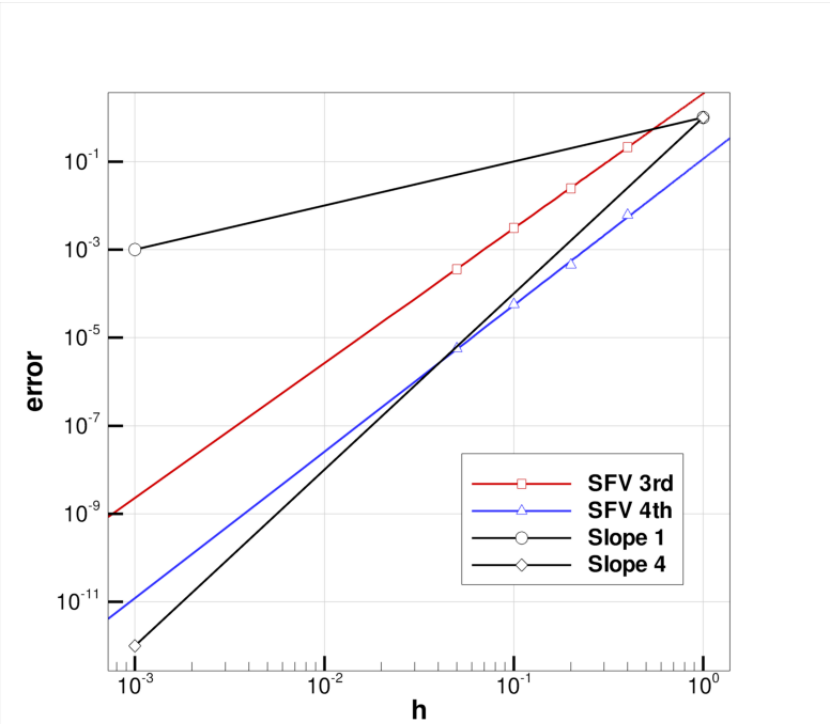

Figure 6. Error versus mesh spacing plot for the Ringleb flow computed with the SFV method.

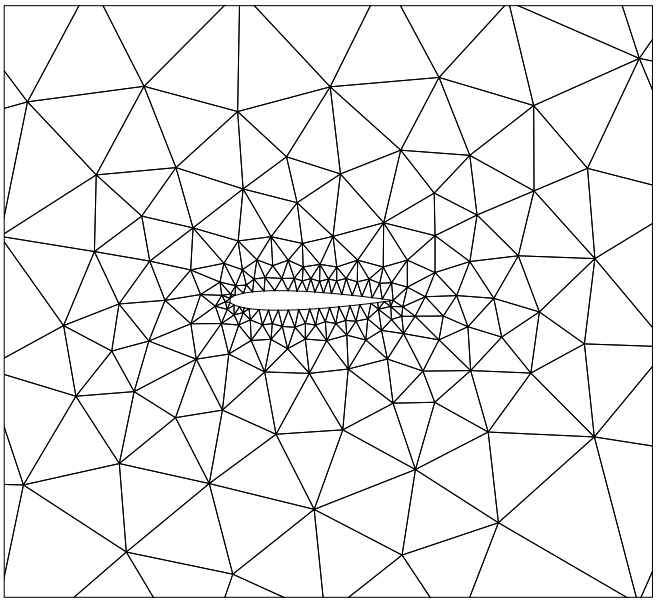

Figure 7. Coarse mesh employed on the NACA 0012 airfoil simulation.

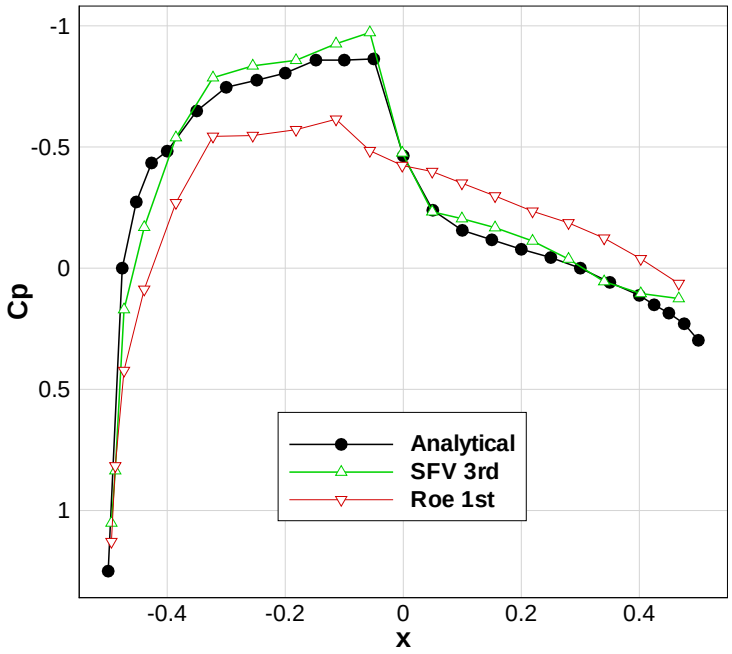

Figure 8. NACA 0012 Cp distribution for coarse mesh solutions.

equations. Figure 9 presents the entropy error generate by the third-order SFV method with linear and curved boundary cells for the coarse mesh, which has only 40 cells to represent the whole airfoil geometry. The curved boundary approach is able to produce the smaller error levels than the linear approach. One can even note, form the figure, that at position $x = 0$ there is an increase of entropy error, due to the presence of the shock wave in this region. This, again, demonstrates that such extension indeed improves the overall accuracy of the SFV method.

6. CONCLUDING REMARKS

The high-order Spectral Finite Volume method is successfully implemented. The method behavior for resolution greater than second order was shown to be in good agreement with both experimental and analytical data. Furthermore, the results obtained are indicative that the current method can yield solutions with similar quality at a much lower computational resource usage than the WENO scheme. The method seems suitable for the aerospace applications in the sense that it is compact, from an implementation point of view, geometry flexible, as it handles unstructured meshes, and computationally efficient.

References

Anderson, W.K., Thomas, J.L. and van Leer, B., 1986. "Comparison of finite volume flux vector splittings for the euler equations". *AIAA Journal*, Vol. 24, No. 9, pp. 1453–1460.

Basso, E., Antunes, A.P. and Azevedo, J.L.F., 2003. "Chimera simulations of supersonic flows over a complex satellite launcher configuration". *Journal of Spacecraft and Rockets*, Vol. 40, No. 3, pp. 345–355.

Breviglieri, C., Azevedo, J., Basso, E. and Souza, M., 2009. "Improved high-order spectral finite volume method implementation for aerodynamic flows". In *27th AIAA Applied Aerodynamics Conference*. AIAA Paper No. 2009-4199, San Antonio, TX.

Breviglieri, C., Basso, E. and Azevedo, J.L.F., 2008. "High-order unstructured spectral finite volume scheme for aerodynamic applications". In *26th AIAA Applied Aerodynamics Conference*. AIAA Paper No. 2008-7182, Honolulu, HI.

Cuthill, E. and McKee, J., 1969. "Reducing the bandwidth of sparse symmetric matrices". In *Proceedings of the 24th National Conference of the ACM*. Brandon Systems Press, New York.

Liou, M.S., 1996. "A sequel to ausm: Ausm+". *Journal of Computational Physics*, Vol. 129, No. 2, pp. 364–382.

Liu, Y., Vinokur, M. and Wang, Z.J., 2006. "Spectral (finite) volume method for conservation laws on unstructured grids v: Extension to three-dimensional systems". *Journal of Computational Physics*, Vol. 212, No. 2, pp. 454–472.

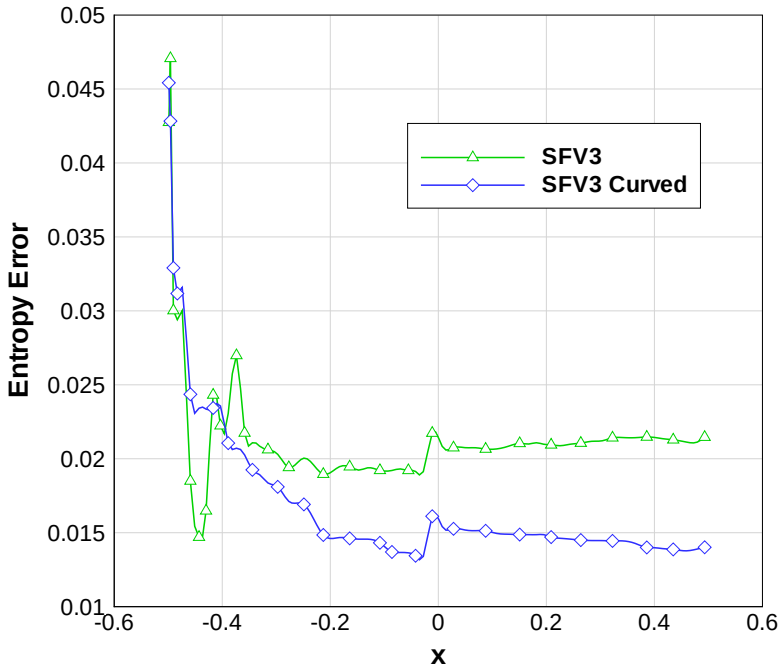

Figure 9. Entropy error for third-order SFV method.

McDevitt, J. and Okuno, A.F., 1985. "Static and dynamic pressure measurements on a naca 0012 airfoil in the ames high reynolds number facility". NASA TP-2485, NASA.

Roe, P.L., 1981. "Approximatte riemann solvers, parameter vectors, and difference schemes". *Journal of Computational Physics*, Vol. 43, No. 2, pp. 357–372.

Sun, Y., Wang, Z.J. and Liu, Y., 2006. "Spectral (finite) volume method for conservation laws on unstructured grids vi: Extension to viscous flow". *Journal of Computational Physics*, Vol. 215, No. 1, pp. 41–58.

van den Abeele, K. and Lacor, C., 2007. "An accuracy and stability study of the 2d spectral volume method". *Journal of Computational Physics*, Vol. 226, No. 1, pp. 1007–1026.

van Leer, B., 1982. "Flux-vector splitting for the euler equations". *Lecture Notes in Physics*, Vol. 170, pp. 507–512.

Wang, Z.J., 2002. "Spectral (finite) volume method for conservation laws on unstructured grids: Basic formulation". *Journal of Computational Physics*, Vol. 178, No. 1, pp. 210–251.

Wang, Z.J. and Liu, Y., 2002. "Spectral (finite) volume method for conservation laws on unstructured grids ii: Extension to two-dimensional scalar equation". *Journal of Computational Physics*, Vol. 179, No. 2, pp. 665–698.

Wang, Z.J. and Liu, Y., 2004. "Spectral (finite) volume method for conservation laws on unstructured grids iii: One-dimensional systems and partition optimization". *Journal of Scientific Computing*, Vol. 20, No. 1, pp. 137–157.

Wang, Z.J. and Liu, Y., 2006. "Extension of the spectral volume method to high-order boundary representation". *Journal of Computational Physics*, Vol. 211, No. 1, pp. 154–178.

Wang, Z.J., Liu, Y. and Zhang, L., 2004. "Spectral (finite) volume method for conservation laws on unstructured grids iv: Extension to two-dimensional systems". *Journal of Computational Physics*, Vol. 194, No. 2, pp. 716–741.

Wolf, W.R. and Azevedo, J.L.F., 2006. "High-order unstructured essentially non oscillatory and weighted essentially non oscillatory schemes for aerodynamic flows". *AIAA Journal*, Vol. 44, No. 10, pp. 2295–2310.

Yang, M. and Wang, Z.J., 2009. "A parameter-free generalized moment limiter for high-order methods on unstructured grids". In *47th AIAA Aerospace Sciences Meeting*. AIAA Paper No. 2009-605, Orlando, FL.

7. Responsibility notice

The authors are the only responsible for the printed material included in this paper